IPPP/09/84
DCPT/09/168
FERMILAB-PUB-09-574-APC
MPP-2009-167
EURONU-WP6-09-10, IDS-NF-013

The multi-channel low energy neutrino factory

Alan Bross and Steve Geer*
Fermi National Accelerator Laboratory, Batavia, IL 60510-0500, USA

Malcolm Ellis
Brunel University, Uxbridge, Middlesex, UB8 3PH, United Kingdom

Enrique Fernández Martínez†
Max-Planck-Institut für Physik (Werner-Heisenberg-Institut), Föhringer Ring 6, 80805 München, Germany

Tracey Li‡ and Silvia Pascoli§
IPPP, Department of Physics, Durham University, Durham, DH1 3LE, United Kingdom

Olga Mena¶
Instituto de Física Corpuscular, IFIC CSIC and Universidad de Valencia, Spain

We show that a low energy neutrino factory with a baseline of 1300 km, muon energy of 4.5 GeV, and either a 20 kton totally active scintillating detector or 100 kton liquid argon detector, can have outstanding sensitivity to the neutrino oscillation parameters θ_{13}, δ and the mass hierarchy. For our estimated exposure of 2.8×10^{23} kton $\times$ decays per muon polarity, the low energy neutrino factory has sensitivity to θ_{13} and δ for $\sin^2(2\theta_{13}) > 10^{-4}$ and to the mass hierarchy for $\sin^2(2\theta_{13}) > 10^{-3}$.

PACS numbers: 14.60.Pq

I. INTRODUCTION

Neutrino oscillations have been robustly established. The present data require two large (θ_{12} and θ_{23}) angles and one small (θ_{13}) angle in the neutrino mixing matrix, and at least two mass squared differences, $\Delta m^2_{ij} \equiv m^2_i - m^2_j$ (where m_i's are the neutrino masses), one driving the atmospheric (Δm^2_{31}) and the other one the solar (Δm^2_{21}) neutrino oscillations. The mixing angles θ_{12} and θ_{23} control the solar and the atmospheric neutrino oscillations, while θ_{13} is the angle which connects the atmospheric and solar neutrino regimes.

A global fit performed at the end of 2008 [1] (see also [2]) provides the following 3σ allowed ranges for the atmospheric mixing parameters: $|\Delta m^2_{31}| = (2.07 - 2.75) \times 10^{-3}$ eV^2 and $0.36 < \sin^2\theta_{23} < 0.67$. The sign of Δm^2_{31} (sign(Δm^2_{31})) cannot be determined from the existing data. The two possibilities, $\Delta m^2_{31} > 0$ or $\Delta m^2_{31} < 0$, correspond to two different types of neutrino mass ordering: normal hierarchy and inverted hierarchy. In addition, information on the octant of θ_{23}, if $\sin^2 2\theta_{23} \neq 1$, is beyond the reach of present experiments. The best fit values for the solar neutrino oscillation parameters are $\Delta m^2_{21} = 7.65 \times 10^{-5}$ eV^2 and $\sin^2\theta_{12} = 0.30$ [1]. A non-zero value of θ_{13} is crucial to enable a measurement of the CP violating phase δ and the mass hierarchy. A combined three-neutrino oscillation analysis of the solar, atmospheric, reactor and long-baseline neutrino data [1] constrains the third mixing angle to be

*Electronic address: sgeer@fnal.gov
†Electronic address: enfmarti@mppmu.mpg.de
‡Electronic address: t.c.li@durham.ac.uk
§Electronic address: silvia.pascoli@durham.ac.uk
¶Electronic address: omena@ific.uv.es

$\sin^2\theta_{13} \leq 0.056$ at the 3σ confidence level, with a best fit value of 0.01. Different analyses undertaken in 2008 using the available solar data from the third phase of the Sudbury Neutrino Observatory (SNO-III) and recent data from KamLAND found a preference for $\sin^2\theta_{13} > 0$ at $\sim 1\sigma$. A similar preference for non-zero θ_{13} was also claimed from Superkamiokande data on atmospheric neutrinos [3] leading to a $\sim 2\sigma$ preference for $\sin^2\theta_{13} > 0$. This second claim is, however, controversial [4]. 2009 data from the MINOS experiment, studying the appearance channel $\nu_\mu \to \nu_e$, also shows a preference for non-zero values of θ_{13} but with an even larger best fit, even more in conflict with the stringent upper bound mainly from the CHOOZ reactor experiment of $\sin^2\theta_{13} \leq 0.056$. A preliminary combination of all the data provides a 1σ range of $\sin^2\theta_{13} = 0.02 \pm 0.01$ [5]. This hint for non-zero θ_{13} and the resulting tension among the different datasets will be probed by the forthcoming generation of accelerator [6, 7] and reactor [8–10] experiments, However, even if the hint for large θ_{13} is confirmed, these experiments lack the power to probe the remaining unknown neutrino oscillation parameters, such as the existence of leptonic CP violation encoded in the phase δ or the ordering of neutrino masses [11]. A new generation of neutrino oscillation experiments is therefore needed for this task or to explore even smaller values of θ_{13} if the present hint is not confirmed.

Future long-baseline experiments will require powerful machines and extremely pure neutrino beams. Among these, neutrino factories [12], in which a neutrino beam is generated from muons decaying within the straight sections of a storage ring, have been shown to be sensitive tools for studying neutrino oscillation physics [12–27].

The neutrino factory exploits the golden signature of the *wrong-sign* muon [12, 13] events, i.e. muons with opposite sign to the muons stored in the neutrino factory. Wrong-sign muons (μ^-) result from $\nu_e \to \nu_\mu$ oscillations (if μ^+ are stored), and can be used to measure the mixing angle θ_{13}, determine the neutrino mass hierarchy, and search for CP violation in the neutrino sector. In addition to the *wrong-sign* muon signal there will also be *right-sign* muon events. These events come from the disappearance muon neutrino channel, $\bar{\nu}_\mu \to \bar{\nu}_\mu$ ($\nu_\mu \to \nu_\mu$), if positive (negative) muons are stored. The discrimination of the *wrong* and *right* sign muons requires the identification of charged current (CC) muon neutrino interactions, and the measurement of the sign of the produced muon. If the interacting neutrinos have energies of more than a few GeV, standard neutrino detector technology, based on large magnetised sampling calorimeters, can be used to measure wrong-sign muons with high efficiency and very low backgrounds. This has been shown to work for neutrino factories with energies of about 20 GeV or greater [16, 18, 28].

Lower energy neutrino factories [24, 27], which store muons with energies < 10 GeV, exploit a fully active calorimeter within a magnet, a detector technology which ensures the detection of lower energy muons. A neutrino factory with muon energies of about 4 GeV has been shown to enable very precise measurements of the neutrino mixing parameters [24, 27]. Electron charge identification also becomes possible in a low energy neutrino factory equipped with a magnetised totally active scintillating detector (TASD) [28]. Therefore, in addition to the wrong and right-sign *muons*, there will also be wrong and right-sign *electrons* from the appearance channel (the *platinum* channel), $\bar{\nu}_\mu \to \bar{\nu}_e$, and the disappearance channel, $\nu_e \to \nu_e$, for positive muons stored in the decay ring [1]. These *platinum* channels, which are the T-conjugates of the golden channels, would provide a possible way of resolving the problem of degenerate solutions [29–32]. It is well known that even a very precise measurement of the appearance probability for neutrinos and antineutrinos at a fixed L/E allows for different solutions of $(\theta_{13}, \mathrm{sign}(\Delta m^2_{31}), \delta)$, severely weakening the sensitivity to these parameters. Many strategies have been advocated to resolve this issue which in general involve another detector [33–38], the combination with another experiment [22, 23, 39–48] and/or the addition of new channels [19, 49].

We will consider the impact of the addition of the platinum channels in the low statistics and high statistics scenarios. We will show that in the case of low statistics, the addition of the platinum channel is vital in enabling the low energy neutrino factory to perform to its full potential, whereas for the high statistics scenario, the platinum channel has little effect - higher statistics combined with complementary information from the different energies of a broad beam alone are sufficient to resolve degeneracies and maximise the performance of the setup.

The structure of the paper is as follows: in Section II we describe the detector capabilities regarding the electron charge identification. In Section III we discuss in detail the physics reach of the proposed setup, which exploits the wrong and right sign muon and electron signals. Based on refined simulations of the detector and on refined designs of the accelerator complex, the decaying muon statistics, detection efficiencies and energy resolution of the detector are improved, providing a more competitive setup with respect to our previous studies [24, 27]. We perform detailed numerical simulations and discuss the sensitivity of the low energy neutrino factory to the mixing angle θ_{13}, to the CP violating phase δ, to the neutrino mass hierarchy, to the octant of the atmospheric mixing angle θ_{23} and to deviations from maximal atmospheric mixing as a function of the energy resolution of the detector and the number of muon decays per year (with and without the addition of the platinum channels). In Section IV we introduce our

[1] Distinguishing the electron signature from the neutral current events will represent a very difficult task for the magnetised calorimeter technology.

preliminary studies of a magnetised 100 kton liquid argon (LAr) detector, comparing its performance to that of the TASD and other near term and future long-baseline neutrino facilities in Section V. Finally, in Section VI, we draw our conclusions.

II. DETECTOR CAPABILITIES: ELECTRON CHARGE IDENTIFICATION

In order to examine the capability of a TASD to correctly determine the charge of an 'electron-like' (electron or positron) track, single positron tracks were generated in a TASD using GEANT4. This first pass at the analysis was done with a visual scan. Positrons were simulated in the baseline TASD with the same dimensions, material and magnetic field as was done in previous studies. Ten events each in momentum bins from 100 MeV/c to 4.9 GeV/c were simulated. The hit positions were smeared and hits were removed to simulate the position reconstruction efficiency. In this study we used a very conservative hit efficiency of only 25%. The remaining, smeared, hit positions were used to produce images for the visual scan. Before the plots were generated, the raw data files were passed through a 'blinder' program which assigned a random event number to the file and chose whether or not to flip the Y axis when making the display. In this way there was no way of knowing if a given event display was of a positive or negative track or from a low, medium or high momentum particle. Each person performing the scan study attempted to determine whether the track curved up or down.

Four scanners were used in this study. In the vast majority of cases, they agreed on the assignment of an event into one of three categories: 1) bends up, 2) bends down, 3) cant tell.

When there was disagreement, the assignment that was most common was taken (this usually meant excluding one scanner's measurement). This visual scan 'reconstruction' was able to correctly determine the charge of the track in about 80% of the events. The charge is correctly identified almost all the time at low momenta. At 3 GeV/c approximately 30% of events are given the wrong sign. Although these results were encouraging, a quantitative determination of the charge misidentification rate and backgrounds was not done in this study. We speculate, however, that for approximately a third of the events, the charge of the positron can be correctly determined with a low expected charge misidentification rate and this assumption is used in some of the simulations that follow.

We arrived at this conclusion from the following arguments: although the electron loses all but $1/e$ of its energy in one radiation length, at the energies of interest the energy loss is through bremsstralung. With a mean free path for photon conversion in plastic scintillator of approximately 33 cm ($7X_0/9$), many of the photons convert far from the vertex (the equivalent of approximately 20 samples). The error on the curvature measurement due to the detector point resolution is

$$\delta\kappa_{res} = \frac{\epsilon}{L^2}\sqrt{\frac{720}{n+4}} \tag{2.1}$$

where ϵ is the detector point resolution of 0.0045 m, L is the effective track length of 33 cm and n the number of samples (20). The error on the curvature is then approximately $(1/\delta\kappa_{res}) \simeq 4$m. With our reference field of 0.5 T and an electron energy of 500 MeV, the radius of curvature is 3.3 m. So given the properties of plastic scintillator and our stated assumptions, it is reasonable to postulate that in $1/e$ of the events the bremsstrahlung photons will convert far enough away from the vertex so that the curvature of the electron (positron) track stub can be determined with a low error rate, as shown in Fig. 1. In Fig. 1a, we show how from just the sigitta of the showering track stub, one would not expect to be able to determine the curvature of the track; however from the entire event structure shown in Fig. 1b, one sees that the positron emitted an energetic photon and the curvature of the remaining track stub is easy to determine visually since the photon conversion is far from the vertex and hits from the conversion do not cause confusion in associating the correct hits to the track stub. This assumption will, of course, need to be verified with a full MC tracking simulation and with input from additional visual scanning studies.

III. PHYSICS REACH: OPTIMISATION OF THE EXPERIMENTAL SETUP

In this section we present the results from numerical simulations of the low energy neutrino factory. We have used the GLoBES software package [50] to simulate several experimental configurations which will be described in the following subsections. These have led us to an optimised setup, which we use unless otherwise specified, defined by the following: the baseline is 1300 km, corresponding to the Fermilab to DUSEL distance. For the beam we consider a muon energy of 4.5 GeV with 1.4×10^{21} useful muon decays per year per polarity, running for ten years (we assume 2×10^7 operational seconds per year, which is twice that of the International Design Study neutrino factory [28]). For the detector we assume a totally active scintillating detector (TASD) with a fiducial mass of 20 kton, energy threshold

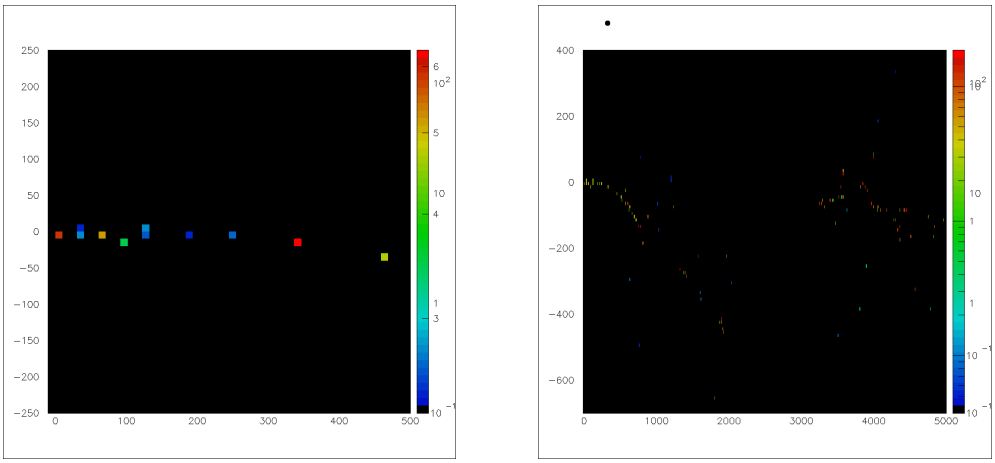

(a) Track stub (b) Entire event

FIG. 1: TASD simulation of a 1.2 GeV positron event. The left panel shows the initial track stub. The right panel shows the entire event with a hard bremsstrahlung photon emitted and an electromagnetic shower on the right.

of 0.5 GeV, energy resolution of 10% with 19 variable-width bins, efficiency for $\mu^{\pm}$ detection of 73% below 1 GeV and 94% above, efficiency for $e^{\pm}$ detection of 37% below 1 GeV and 47% above, and a background level of 10^{-3} on the $\nu_e \to \nu_\mu$ ($\bar{\nu}_e \to \bar{\nu}_\mu$) and $\nu_\mu \to \nu_\mu$ ($\bar{\nu}_\mu \to \bar{\nu}_\mu$) channels and 10^{-2} on the $\nu_\mu \to \nu_e$ ($\bar{\nu}_\mu \to \bar{\nu}_e$) channels. We assume that the background to each channel arises predominantly from charge misidentification and neutral current events, modeling the background to each channel as a constant fraction of the rates of the wrong-sign and neutral current channels.

We assume the same oscillation parameters as in [51]: $\sin^2\theta_{12} = 0.3$, $\theta_{23} = \pi/4$, $\Delta m^2_{21} = 8.0 \times 10^{-5}$ eV^2, and $|\Delta m^2_{31}| = 2.5 \times 10^{-3}$ eV^2 with a 10% uncertainty on the atmospheric parameters, 4% uncertainty on the solar parameters, and 2% uncertainty on the matter density. In all our simulations we have used the exact oscillation probabilities, taking into account matter effects, and have marginalised over all parameters.

The most significant alteration relative to our previous setup [24, 27] consists of the addition of the $\nu_\mu \to \nu_e$ and $\bar{\nu}_\mu \to \bar{\nu}_e$ channels. These *platinum* channels are the T-conjugates of the golden channels ($\nu_e \to \nu_\mu$, $\bar{\nu}_e \to \bar{\nu}_\mu$), and we will demonstrate the power of this unique combination to reduce the degeneracies in the θ_{13}, δ and sign(Δm^2_{31}) parameter space. It has already been established that the elimination of these degenerate solutions might require additional information from a second baseline and detector [19, 33–38], or from a complementary experiment [22, 23, 39–48].

We choose instead to exploit the ability of the TASD to detect and identify the charge of e^- and e^+, which gives us access to the platinum channel. The probability for this channel, to leading order in the small quantities θ_{13}, $\alpha = \Delta m^2_{21}/\Delta m^2_{31}$ and $EA/\Delta m^2_{31}$ (where $A = \sqrt{2} G_F n_e$ is the matter potential and n_e is the electron number density), is identical to that for the golden channel [16] with the interchange of $\delta \to -\delta$ and is shown below.

$$P_{\mu e} = s^2_{213} s^2_{23} \sin^2\left(\frac{\Delta m^2_{31} L}{4E} - \frac{AL}{2}\right) \tag{3.1}$$

$$+ \alpha s_{213} s_{212} s_{223} \frac{\Delta m^2_{31}}{2EA} \sin\left(\frac{AL}{2}\right) \sin\left(\frac{\Delta m^2_{31} L}{4E} - \frac{AL}{2}\right) \cos\left(\frac{\Delta m^2_{31} L}{4E} - \delta\right) \tag{3.2}$$

$$+ \alpha^2 c^2_{23} s^2_{212} \left(\frac{\Delta m^2_{31}}{2EA}\right)^2 \sin^2\left(\frac{AL}{2}\right) \tag{3.3}$$

$$P_{e\mu} = s^2_{213} s^2_{23} \sin^2\left(\frac{\Delta m^2_{31} L}{4E} - \frac{AL}{2}\right) \tag{3.4}$$

$$+ \alpha s_{213} s_{212} s_{223} \frac{\Delta m^2_{31}}{2EA} \sin\left(\frac{AL}{2}\right) \sin\left(\frac{\Delta m^2_{31} L}{4E} - \frac{AL}{2}\right) \cos\left(\frac{\Delta m^2_{31} L}{4E} + \delta\right) \tag{3.5}$$

$$+ \alpha^2 c^2_{23} s^2_{212} \left(\frac{\Delta m^2_{31}}{2EA}\right)^2 \sin^2\left(\frac{AL}{2}\right) \tag{3.6}$$

We use a notation where $s_{ij} = \sin\theta_{ij}$, $s_{2ij} = \sin(2\theta_{ij})$, $c_{ij} = \cos\theta_{ij}$, $c_{2ij} = \cos(2\theta_{ij})$, E is the neutrino energy and L is the baseline. The first line of each probability, subequations (3.1) and (3.4), is the *atmospheric term* which is quadratic in $\sin(2\theta_{13})$ and will be dominant in the scenario that θ_{13} is large ($\sin^2(2\theta_{13}) \gtrsim 10^{-2}$), and at high energies. The atmospheric term provides sensitivity to θ_{13}, the mass hierarchy, and is sensitive to the octant of θ_{23}. The second line, subequations (3.2) and (3.5), is the *CP term* which is linear in $\sin(2\theta_{13})$ and dominates for intermediate values of θ_{13} if $\delta \neq 0$ or π. The dependence on δ enters via the oscillatory cosine term which can take either a positive or negative sign depending on the value of the phase. This can lead to constructive or destructive interference between the atmospheric and CP terms, meaning that sensitivities to θ_{13} and the mass hierarchy are strongly dependent on the value of δ. Due to the inverse dependence on energy, the CP term becomes most visible at lower energies; therefore it is important to have access to the second oscillation maximum to establish if CP is violated. Thus a shorter baseline/ lower energy is desirable to enable a clean measurement of δ, whereas a higher energy and, especially, a long-baseline, guarantees sensitivity to the mass hierarchy. The low energy neutrino factory is unique in having a surprising degree of sensitivity to the mass hierarchy in spite of its low energy (as we show in Section III C) due to its multitude of channels with high statistics and good background rejection, and due to the broad spectrum that includes energies beyond the first oscillation peak, thus enabling complementary information to be obtained to solve degeneracies. The third line, subequations (3.3) and (3.6), is the *solar term* which is independent of θ_{13}, δ and the mass hierarchy, and is dominant in the case that θ_{13} is very small ($\sin^2(2\theta_{13}) \lesssim 10^{-4}$). In this regime, measurements will be extremely challenging and a high energy neutrino factory may be the only option [16, 18, 28].

If we consider the fact that the probability for the CP-conjugated golden channel, $\bar{\nu}_e \to \bar{\nu}_\mu$, takes a similar form to that of the golden channel but with the substitutions $\delta \to -\delta$ and $A \to -A$ and that the CPT-conjugated golden channel is identical to the golden channel, with the exchange of $A \to -A$, we can understand the complementarity of these four channels: each of the channels has a different dependence on the parameters θ_{13}, δ and $\text{sign}(\Delta m^2_{31})$ and so degenerate solutions are present at *different* points in the parameter space for each of the channels. Thus the degenerate solutions from one channel can be eliminated by the information from another channel.

We will mention briefly that the ability of the TASD to detect electrons also enables measurement of the ν_e ($\bar{\nu}_e$) disappearance channel:

$$P_{\nu_e \to \nu_e} \approx 1 - s^2_{213} \sin^2\left(\frac{\Delta m^2_{31} L}{4E} - \frac{AL}{2}\right). \tag{3.7}$$

However, as this channel is CP-invariant and has only weak dependence on the mass hierarchy, it is expected and has been verified that its addition does not provide any significant improvement.

In the rest of this section we now show the impact of our improved statistics and energy resolution, and of the addition of the platinum channels.

A. Energy resolution

Firstly we illustrate how our more optimistic estimate of 10% for the energy resolution, dE/E, improves the performance of our setup. In Fig. 2 we show how the new resolution improves upon the old value of 30% (with nine variable width bins) for $\theta_{13} = 1^\circ$ and 5°. We observe that in addition to the significant increase in sensitivity to θ_{13} and δ, the hierarchy degeneracy is now almost completely eliminated even for small values of θ_{13}.

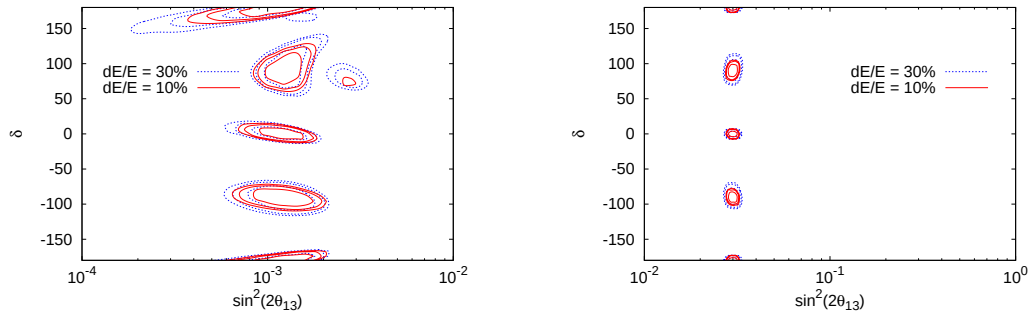

(a) $\theta_{13} = 1^\circ$ (b) $\theta_{13} = 5^\circ$

FIG. 2: Comparing an energy resolution of $dE/E = 30\%$ (dotted blue lines) and 10% (solid red lines): 68%, 90% and 95% confidence level contours in the $\sin^2(2\theta_{13}) - \delta$ plane for true values of $\delta = -180^\circ, -90^\circ, 0^\circ$ and 90° and a) $\theta_{13} = 1^\circ$, b) $\theta_{13} = 5^\circ$.

B. Inclusion of the platinum channel

We define *Scenario 1* to be the one in which only $\mu^{\pm}$ detection is possible, giving us access to only the ν_μ and $\bar{\nu}_\mu$ appearance and disappearance channels. In *Scenario 2* it is also possible to detect $e^{\pm}$ and hence exploit the additional information from the ν_e and $\bar{\nu}_e$ appearance channels. To illustrate the power of the addition of the platinum channel to our setup, in Fig. 3 we compare the sensitivities of the two scenarios when using a muon decay rate of 5.0×10^{20} (left column) and 1.4×10^{21} (right column) per year, varying the background level of the ν_e ($\bar{\nu}_e$) appearance channel from a hypothetical zero (top row) to 10^{-2} (bottom row).

In the case of the lower statistics, we observe that the addition of the platinum channel with zero background produces a drastic improvement in sensitivity to all parameters. For a background of 10^{-2} the improvement is smaller but still visible, especially for resolving the hierarchy degeneracy (see [49]). At higher backgrounds we find that this gain is almost lost. In the case of the high statistics, we observe a smaller improvement for zero background, which becomes insignificant, apart from a slight resolution of the mass hierarchy, at a background level of 10^{-2}. Thus we conclude that since the estimated background on the ν_e ($\bar{\nu}_e$) appearance channels will be $\sim 10^{-2}$, the platinum channel will be crucial in maximising the physics reach of our setup if statistics are limited to 5.0×10^{20} useful muon decays per year, whereas it will be less important but still aids in the determination of the mass hierarchy for the higher statistics scenario.

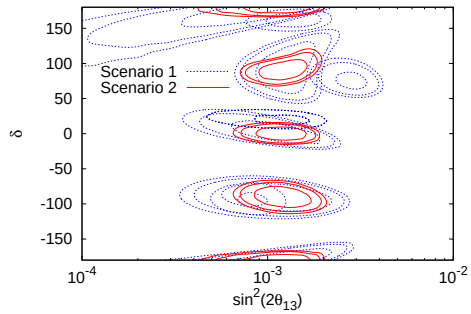

(a) 5.0×10^{20} decays per year, zero background

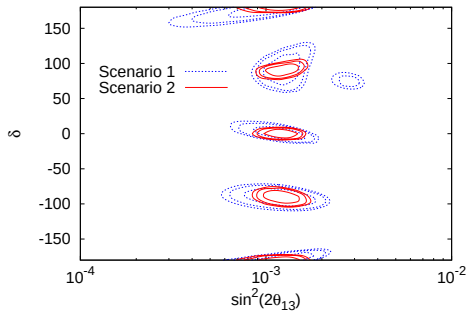

(b) 1.4×10^{21} decays per year, zero background

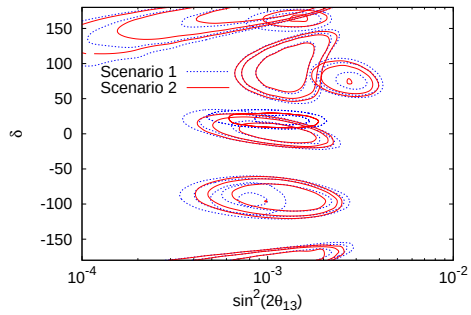

(c) 5.0×10^{20} decays per year, 10^{-2} background

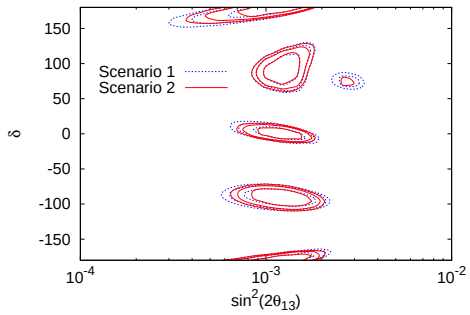

(d) 1.4×10^{21} decays per year, 10^{-2} background

FIG. 3: Comparison of Scenario 1 (ν_μ ($\bar{\nu}_\mu$) appearance and disappearance only - dotted blue lines), and Scenario 2 (ν_e ($\bar{\nu}_e$) appearance included - solid red lines) when using 5.0×10^{20} $\mu^{\pm}$ decays per year (left) or 1.4×10^{21} decays per year (right), and a background of zero (top row) or 10^{-2} (bottom row) on the ν_e ($\bar{\nu}_e$) channels: 68%, 90% and 95% confidence level contours in the $\sin^2(2\theta_{13}) - \delta$ plane, for $\delta = -180°, -90°, 0°$ and $90°$ and $\theta_{13} = 1°$.

C. Results

Here we present the results of our optimisation studies, in terms of 3σ θ_{13} discovery potential, CP discovery potential, and sensitivity to the mass hierarchy in the $\sin^2(2\theta_{13}) - \delta$ plane (Fig. 4). In addition we also consider the 3σ sensitivity to θ_{23} in the $\sin^2(2\theta_{13}) - \sin\theta_{23}$ plane, both in terms of the ability to exclude a maximal value of θ_{23}

(Fig. 5a) and to identify the octant of θ_{23} (Fig. 5b). The results from our optimised setup described in Section III are shown by the solid green lines; we have also considered a setup where only the statistics are altered, to 2.8×10^{21} decays per year (solid red lines), and a setup where only the muon energy is increased to 6.0 GeV (dashed blue lines). From this we demonstrate that for all the observables considered, doubling the flux is always preferable to an increase in energy.

For θ_{13} discovery potential, CP discovery potential and θ_{23} sensitivity we only show the results for a normal hierarchy, having verified that similar results are obtained for an inverted hierarchy. We have assumed in Fig. 5 (θ_{23} sensitivity) a value of $\delta = 90°$ although we have also studied other values of δ and find no strong dependence on the CP phase, since sensitivity to θ_{23} is mainly obtained from terms with no dependence on δ in the oscillation probabilities discussed in Section III. For the exclusion of $\theta_{23} = 45°$, an upward curve is seen for large θ_{13}. This can be understood because the addition of a large θ_{13} to the ν_μ disappearance probability introduces an asymmetry in θ_{23} that shifts the contours to larger values (see eq. (1) and Fig. 8 of Ref. [52]).

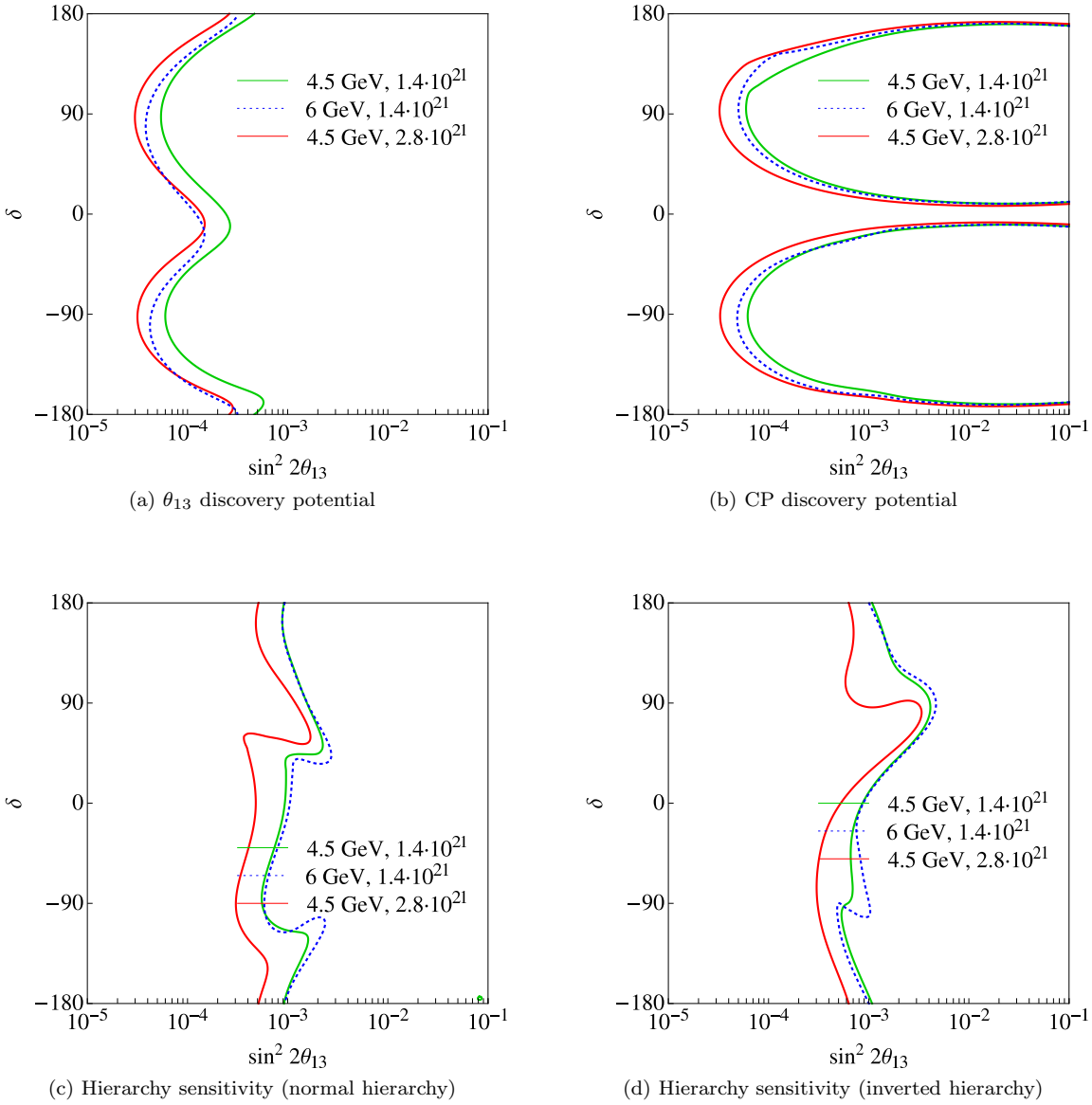

(a) θ_{13} discovery potential

(b) CP discovery potential

(c) Hierarchy sensitivity (normal hierarchy)

(d) Hierarchy sensitivity (inverted hierarchy)

FIG. 4: 3σ confidence level contours in the $\sin^2(2\theta_{13}) - \delta$ plane for a) θ_{13} discovery potential, b) CP discovery potential, c) hierarchy sensitivity (for true normal hierarchy), d) hierarchy sensitivity (inverted hierarchy).

We note that this setup has remarkable sensitivity to θ_{13} and δ for values of $\sin^2(2\theta_{13}) > 10^{-4}$, and that its sensitivity to the mass hierarchy is an order of magnitude better that that of other proposed experiments exploiting the same baseline e.g. the wide-band beam experiment in [53]. We can attribute these qualities to our setup's unique

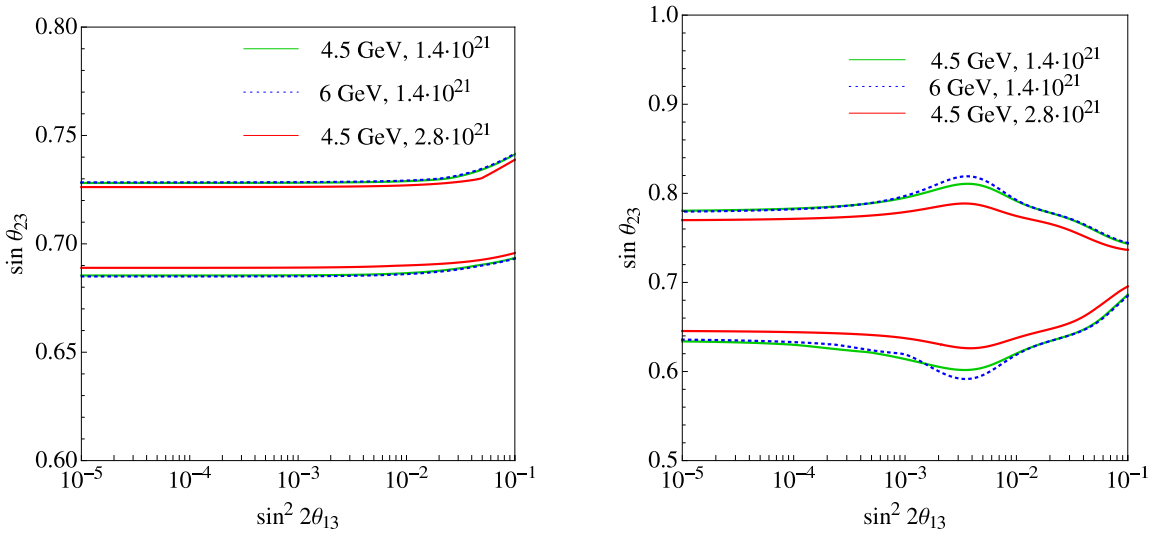

(a) Sensitivity to $\theta_{23} \neq 45°$

(b) Sensitivity to the θ_{23} octant

FIG. 5: 3σ allowed regions in the $\sin^2(2\theta_{13}) - \sin\theta_{23}$ plane for a) potential to exclude $\theta_{23} = 45°$, b) sensitivity to the θ_{23} octant.

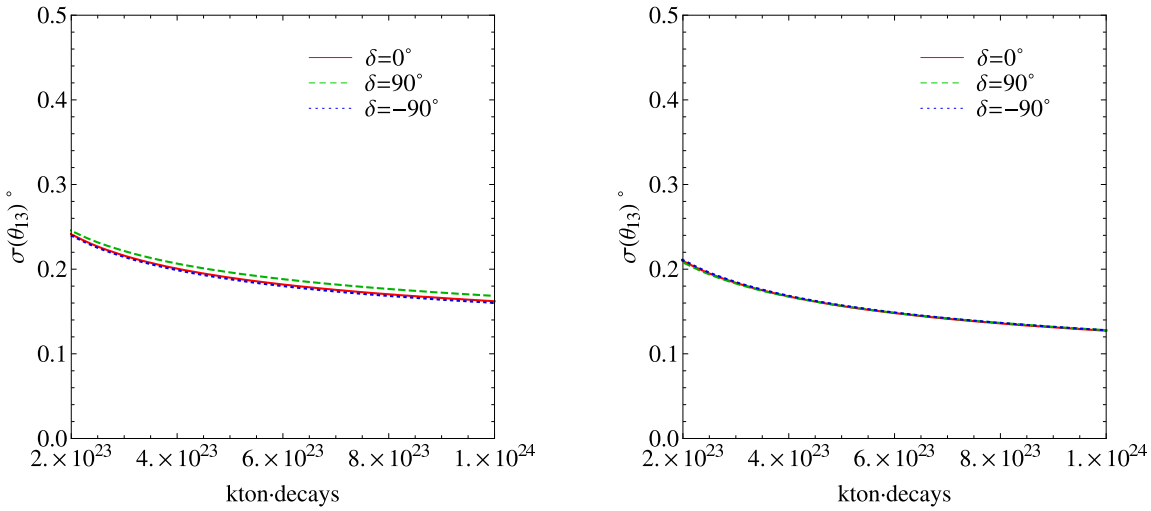

(a) Sensitivity to θ_{13}, including systematic errors and backgrounds

(b) Sensitivity to θ_{13}, no systematic errors and backgrounds

FIG. 6: 1σ error in the measurement of the θ_{13} mixing angle for a simulated value of $\theta_{13} = 5°$ and different values of the CP violating phase δ when a) including systematic errors and backgrounds, b) no systematic errors and backgrounds are included.

combination of high statistics and good background rejection coupled with an intermediate baseline, allowing for a clean measurement of the CP phase whilst also allowing for the mass hierarchy to be determined for $\sin^2(2\theta_{13}) > 10^{-3}$.

We have also explored how the precision with which θ_{13}, δ and the deviation from maximal θ_{23} could eventually be measured at the low energy neutrino factory varies as a function of exposure (detector mass $\times$ decays) per polarity. Our standard setup corresponds to 20 kton $\times$ 1.4×10^{21} decays/ year $\times$ 10 years $= 2.8 \times 10^{23}$ kton $\times$ decays per polarity. We find that if the mixing angle θ_{13} turns out to be large, the unknown leptonic mixing parameters could be measured with unprecedented precision at a future low energy neutrino factory for sufficiently high exposures. The gain in precision is much less pronounced for values larger than 6×10^{23} kton $\times$ decays per polarity, hence it may not be worth trying to increase the exposure beyond that value.

Fig. 6a shows the 1σ error expected in the measurement of the mixing angle θ_{13} at a future low energy neutrino factory as a function of the exposure (in kton $\times$ decays) per polarity, assuming that nature has chosen $\theta_{13} = 5°$. The dependence of these results on the value of the CP violating phase is very mild. The 1σ error in the extraction of θ_{13} when no backgrounds and no systematic errors are included in the analysis is illustrated in Fig. 6b. Comparing the

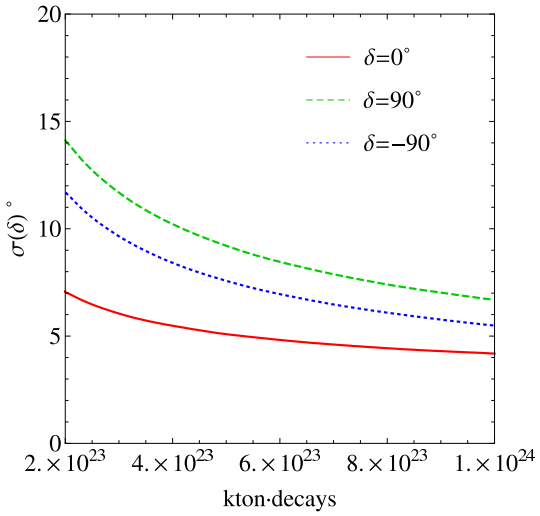

(a) Sensitivity to δ, including systematic errors and backgrounds

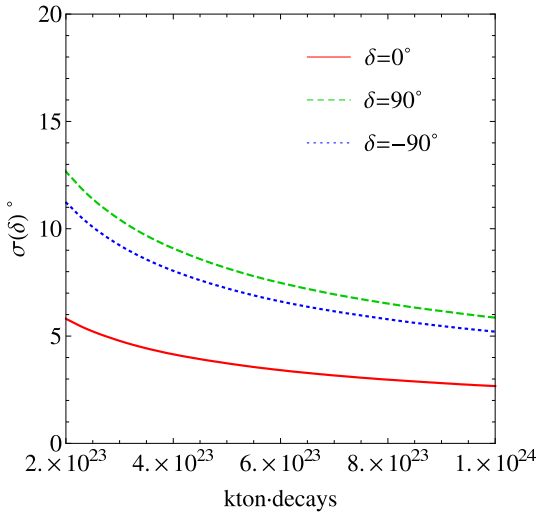

(b) Sensitivity to δ, no systematic errors and backgrounds

FIG. 7: 1σ error in the measurement of the CP violating phase δ for a simulated value of $\theta_{13} = 5^\circ$ and different values of the CP violating phase δ when a) including systematic errors and backgrounds, b) no systematic errors and backgrounds are included.

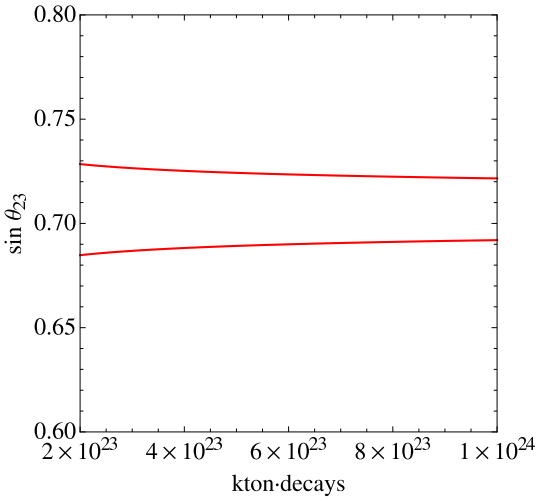

(a) Sensitivity to $\theta_{23} \neq 45^\circ$, including systematic errors and backgrounds

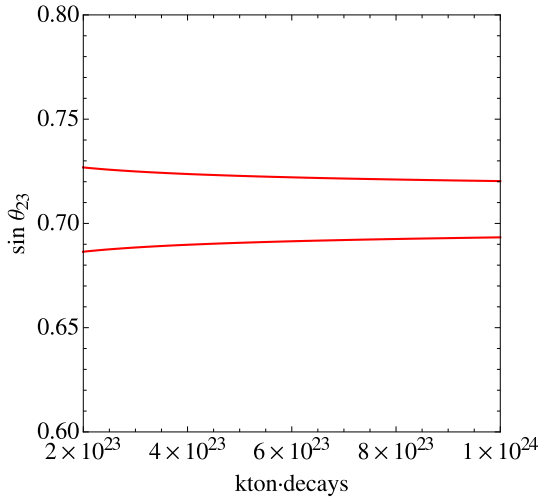

(b) Sensitivity to $\theta_{23} \neq 45^\circ$, no systematic errors and backgrounds

FIG. 8: 3σ regions for which maximal θ_{23} can be excluded, using a simulated value of $\theta_{13} = 0^\circ$ when a) including systematic errors and backgrounds, b) no systematic errors and backgrounds are included.

two panels we observe that non-zero systematics and backgrounds effectively halve the exposure.

Fig. 7a shows the 1σ error expected in the measurement of the CP phase δ as a function of the exposure for a simulated value $\theta_{13} = 5^\circ$, for different values of the CP violating phase δ. The results are highly dependent on the value of the CP violating phase, as expected. For $\delta = 90^\circ$, there are strong correlations with θ_{13}, as can be seen from Fig. 3, and therefore the error in the measurement of the CP violating phase is larger. The 1σ error in the extraction of δ when no backgrounds and no systematic errors are included in the analysis is illustrated in Fig. 7b. Switching off systematic errors and backgrounds has a larger impact for the $\delta = 0^\circ$ case, again effectively halving the exposure, since correlations among δ and θ_{13} are negligible when $\delta = 0^\circ$ and the precision is more limited by the background and systematic errors instead.

We also explore the sensitivity to maximal mixing, i.e. the ability to exclude $\theta_{23} = 45^\circ$, versus the exposure. We present the 3σ results in Fig. 8. We have used a simulated value of $\theta_{13} = 0^\circ$ here (so that δ is irrelevant) as the sensitivity to θ_{23} maximality comes primarily from the ν_μ ($\bar{\nu}_\mu$) disappearance channels which are not dependent on

θ_{13}. Since the disappearance channels are also not strongly dependent upon systematic errors or backgrounds, there is little change obtained by switching these off.

IV. PRELIMINARY SIMULATIONS OF A 100 KTON LIQUID ARGON DETECTOR

Recently there has been much interest in the possibility of constructing a kton-scale liquid argon (LAr) detector [54]. If such a detector can be magnetised, it could be utilised in combination with a low energy neutrino factory and we have performed some preliminary studies to assess the potential of a 100 kton LAr detector for this experiment. As the design of large LAr detectors is still in the early stages, there are large uncertainties in the estimates for the detector performance. We assume an efficiency of 80% on all channels and 5% energy resolution for quasi-elastic events, then consider a range of values for other parameters. In the most conservative scenario, we assume 5% systematics, 20% energy resolution for non quasi-elastic events, and backgrounds of 5×10^{-3} on the ν_μ ($\bar{\nu}_\mu$) (dis)appearance channels and 0.8 on the ν_e ($\bar{\nu}_e$) appearance channels [55]. For the optimistic scenario we use values identical to the TASD: 2% systematics, 10% energy resolution for non quasi-elastic events, and backgrounds of 1×10^{-3} on the ν_μ ($\bar{\nu}_\mu$) (dis)appearance channels and 1×10^{-2} on the ν_e ($\bar{\nu}_e$) appearance channels. We find that varying the systematics, energy resolution and ν_e ($\bar{\nu}_e$) background do not play a large role in altering the results; the dominant effect comes from the variation of the ν_μ ($\bar{\nu}_\mu$) background. We show our results, taking into account these ranges, in Fig. 9.

V. COMPARISON WITH OTHER EXPERIMENTS

Finally, the results of the low energy neutrino factory with both the TASD and LAr detector are compared with other long-baseline experiments in Fig. 9. We show the 3σ results for θ_{13} discovery, CP discovery potential, and hierarchy sensitivity (for normal hierarchy only) as a function of $\sin^2(2\theta_{13})$ in terms of the CP fraction. In order to make a fair comparison, we have used half the flux described in Section III for the low energy neutrino factory, to make it consistent with the other experiments which assume only 10^7 seconds per year of observation. However, we believe that the fluxes in Section III are feasible. The results from the TASD are shown by the red line and those from the LAr detector are shown by the blue band. The right-hand edge of the band corresponds to the conservative estimate of the detector performance, and the left-hand edge to the most optimistic estimate. As the optimistic scenario assumes an almost identical performance to the TASD, the left-hand edge of the blue band also corresponds to the results obtainable from a 100 kton TASD. Results from the high energy neutrino factory [28], T2HK [56], wide-band beam [53], 100γ β-beam [57], 350γ β-beam [58] and 4-ion β-beam [59] are also shown.

In terms of sensitivity to θ_{13}, a conservative low energy neutrino factory is an order of magnitude less sensitive than the high energy neutrino factory, but is still competitive with the β-beam experiments, giving an approximately equal performance to the 4-ion β-beam (which requires two baselines to resolve the degeneracy problem, as for the high energy neutrino factory). However, the performance of an aggressive low energy neutrino factory setup surpasses that of all other experiments except for the high energy neutrino factory. For CP violation, the low energy neutrino factory gives remarkable results: the most optimistic setup outperforms the high energy neutrino factory for all values of θ_{13}, and even the most conservative setup gives superior performance for $\sin^2(2\theta_{13}) > 2 \times 10^{-3}$, again equaling that of the 4-ion β-beam. For sensitivity to the mass hierarchy, the low energy neutrino factory gives an improvement over all other experiments apart from the higher energy setup and the 4-ion β-beam with their challenging 7000 km baseline.

VI. CONCLUSIONS

We have optimised a low energy neutrino factory setup with a baseline of 1300 km, defining a reference setup to be one with a muon energy of 4.5 GeV with 1.4×10^{21} useful muon decays per year, per polarity, running for ten years. For the detector we assume a totally active scintillating detector (TASD) with a fiducial mass of 20 kton, energy threshold of 0.5 GeV, energy resolution of 10%, efficiency for $\mu^\pm$ detection of 73% below 1 GeV and 94% above, efficiency for $e^\pm$ detection of 37% below 1 GeV and 47% above, and a background level of 10^{-3} on the $\nu_e \to \nu_\mu$ ($\bar{\nu}_e \to \bar{\nu}_\mu$) and $\nu_\mu \to \nu_\mu$ ($\bar{\nu}_\mu \to \bar{\nu}_\mu$) channels and 10^{-2} on the $\nu_\mu \to \nu_e$ ($\bar{\nu}_\mu \to \bar{\nu}_e$) channels. We have also considered a 100 kton liquid argon detector and found that its performance would equal or surpass that of the 20 kton TASD.

We have demonstrated how improving the energy resolution and statistics improves the performance of the setup, showing that high statistics play a vital role. We have also shown how the unique combination of golden and platinum channels is a powerful way of resolving degeneracies in the case of limited statistics.

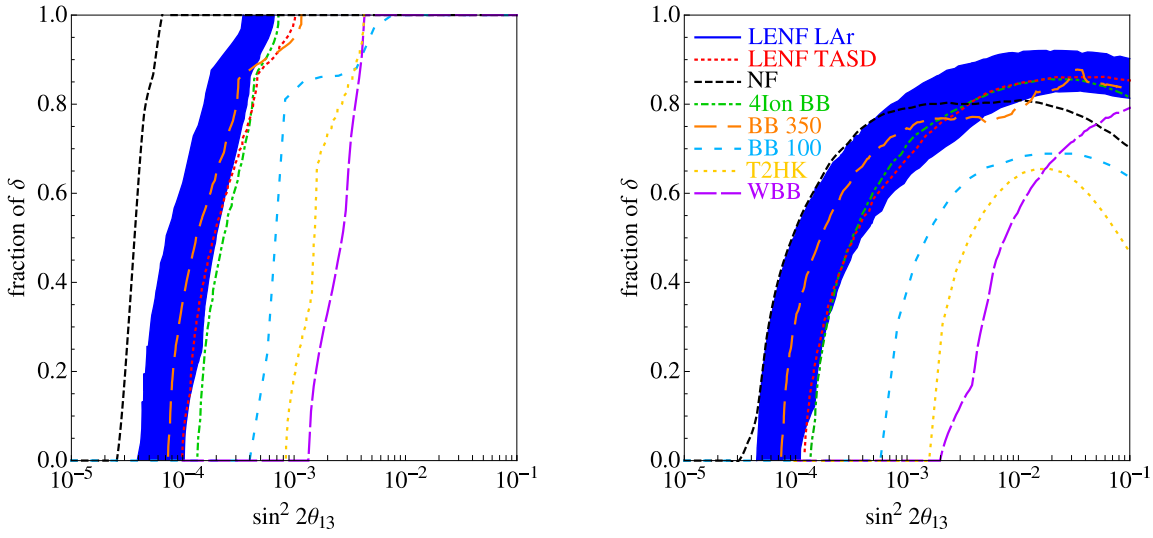

(a) θ_{13} discovery potential

(b) CP discovery potential

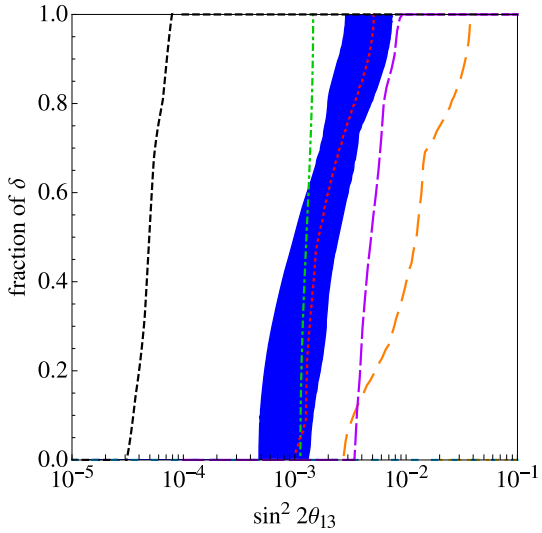

(c) Hierarchy sensitivity

FIG. 9: Comparison of 3σ allowed contours for the low energy neutrino factory with 20 kton TASD (red line) and 100 kton LAr detector (blue band), the high energy neutrino factory (black line), T2HK (yellow line), the wide-band beam (purple line) and three β-beams (green, orange, light blue lines) for a) θ_{13} discovery potential, b) CP discovery potential, c) hierarchy sensitivity.

Using our optimised setup, the low energy neutrino factory can have sensitivity to θ_{13} and δ for $\sin^2(2\theta_{13}) > 10^{-4}$, competitive with the high neutrino factory. Sensitivity to the mass hierarchy is accessible for $\sin^2(2\theta_{13}) > 10^{-3}$, better than other experiments using the same baseline due to the complementarity of measurements with different channels and different energies. Even if the flux is halved to equal that of other long-baseline experiments, the low energy neutrino factory is still competitive, performing especially well for CP discovery at large values of θ_{13}. We have also studied the sensitivity to θ_{23}, finding that it is possible to exclude maximal θ_{23} at 3σ for $\theta_{23} \lesssim 43°$ and $\theta_{23} \gtrsim 47°$, roughly independent of θ_{13}, and to identify the octant for $\theta_{23} \lesssim 37°$ and $\theta_{23} \gtrsim 53°$.

Studies of the sensitivities as a function of exposure (detector mass × number of decays) show that the effect of non-zero systematic errors and backgrounds is to effectively halve the exposure, affecting the sensitivity to θ_{13}, δ (especially for $\delta = 0°$) and θ_{23}. For exposures $> 6 \times 10^{23}$ kton × decays per polarity and large θ_{13}, the low energy neutrino factory could measure the oscillation parameters with unprecedented precision.

We conclude that the low energy neutrino factory has excellent sensitivity to the standard oscillation parameters and is therefore a potential candidate for a next-generation long-baseline experiment.

Acknowledgments

This work was supported in part by the Fermi National Accelerator Laboratory, which is operated by the Fermi Research Association, under Contract No. DE-AC02-76CH03000 with the U.S. Department of Energy. SP and TL acknowledge the support of EuCARD (European Coordination for Accelerator Research and Development), which is co-funded by the European Commission within the Framework Programme 7 Capacities Specific Programme, under Grant Agreement number 227579. OM and SP would like to thank the Theoretical Physics Department at Fermilab for hospitality and support. TL also acknowledges the support of a STFC studentship and funding for overseas fieldwork. EFM acknowledges support by the DFG cluster of excellence 'Origin and Structure of the Universe'. This work was undertaken with partial support from the European Community under the European Commission Framework Programme 7 Design Studies: EUROnu (Project Number 212372) and LAGUNA (Project Number 212343). The EC is not liable for any use that may be made of the information contained herein.

[1] T. Schwetz, M. A. Tortola and J. W. F. Valle, New J. Phys. **10**, 113011 (2008).
[2] M. C. Gonzalez-Garcia and M. Maltoni, Phys. Rept. **460**, 1 (2008).
[3] G. L. Fogli, E. Lisi, A. Marrone, A. Palazzo and A. M. Rotunno, Phys. Rev. Lett. **101**, 141801 (2008).
[4] M. Maltoni and T. Schwetz, arXiv:0812.3161 (hep-ph).
[5] G. L. Fogli, E. Lisi, A. Marrone, A. Palazzo and A. M. Rotunno, arXiv:0905.3549 (hep-ph).
[6] Y. Itow *et al.*, arXiv:hep-ex/0106019.
[7] D. S. Ayres *et al.* [NOvA Collaboration], arXiv:hep-ex/0503053.
[8] F. Ardellier *et al.*, arXiv:hep-ex/0405032; F. Ardellier *et al.* [Double Chooz Collaboration], arXiv:hep-ex/0606025.
[9] X. Guo *et al.* [Daya Bay Collaboration], arXiv:hep-ex/0701029.
[10] Information about the experiment available at *http://neutrino.snu.ac.kr/RENO*.
[11] P. Huber, M. Lindner, T. Schwetz and W. Winter, arXiv:0907.1896 (hep-ph).
[12] S. Geer, Phys. Rev. D **57**, 6989 (1998) [Erratum-ibid. D **59**, 039903 (1999)].
[13] A. De Rujula, M. B. Gavela and P. Hernandez, Nucl. Phys. B **547**, 21 (1999).
[14] V. D. Barger, S. Geer and K. Whisnant, Phys. Rev. D **61**, 053004 (2000); A. Donini *et al.*, Nucl. Phys. B **574**, 23 (2000); V. D. Barger *et al.*, Phys. Rev. D **62**, 073002 (2000).
[15] V. D. Barger *et al.*, Phys. Rev. D **62**, 013004 (2000).
[16] A. Cervera, *et al.*, Nucl. Phys. B **579**, 17 (2000) [Erratum-ibid. B **593**, 731 (2001)].
[17] M. Freund, P. Huber and M. Lindner, Nucl. Phys. B **585**, 105 (2000); V. D. Barger *et al.*, Phys. Lett. B **485**, 379 (2000); J. Burguet-Castell *et al.*, Nucl. Phys. B **608**, 301 (2001); M. Freund, P. Huber and M. Lindner, Nucl. Phys. B **615**, 331 (2001).
[18] C. Albright *et al.*, arXiv:hep-ex/0008064.
[19] A. Donini, D. Meloni and P. Migliozzi, Nucl. Phys. B **646**, 321 (2002); D. Autiero *et al.*, Eur. Phys. J. C **33**, 243 (2004).
[20] A. Blondel *et al.*, Nucl. Instrum. Meth. A **451**, 102 (2000); M. Apollonio *et al.*, arXiv:hep-ph/0210192.
[21] C. Albright *et al.* [Neutrino Factory/Muon Collider Collaboration], arXiv:hep-ph/0411123.
[22] O. Mena, Mod. Phys. Lett. A **20**, 1 (2005).
[23] P. Huber, M. Lindner, M. Rolinec and W. Winter, Phys. Rev. D **74**, 073003 (2006).
[24] S. Geer, O. Mena and S. Pascoli, Phys. Rev. D **75**, 093001 (2007).
[25] P. Huber and W. Winter, arXiv:0706.2862 (hep-ph).
[26] O. Mena, arXiv:0809.4829 (hep-ph).
[27] A. D. Bross, M. Ellis, S. Geer, O. Mena and S. Pascoli, Phys. Rev. D **77**, 093012 (2008).
[28] The International Scoping Study for a Neutrino Factory, RAL-TR-2007-24.
[29] G. L. Fogli and E. Lisi, Phys. Rev. D **54**, 3667 (1996).
[30] H. Minakata and H. Nunokawa, JHEP **0110**, 001 (2001).
[31] V. D. Barger, S. Geer, R. Raja and K. Whisnant, Phys. Rev. D **63**, 113011 (2001).
[32] T. Kajita, H. Minakata and H. Nunokawa, Phys. Lett. B **528**, 245 (2002); H. Minakata, H. Nunokawa and S. J. Parke, Phys. Rev. D **66**, 093012 (2002); P. Huber, M. Lindner and W. Winter, Nucl. Phys. B **645**, 3 (2002); A. Donini, D. Meloni and S. Rigolin, JHEP **0406**, 011 (2004); M. Aoki, K. Hagiwara and N. Okamura, Phys. Lett. B **606**, 371 (2005); O. Yasuda, New J. Phys. **6**, 83 (2004); O. Mena and S. J. Parke, Phys. Rev. D **72**, 053003 (2005).
[33] H. Minakata and H. Nunokawa, Phys. Lett. B **413**, 369 (1997).
[34] V. Barger, D. Marfatia and K. Whisnant, Phys. Rev. D **66**, 053007 (2002).
[35] O. Mena Requejo, S. Palomares-Ruiz and S. Pascoli, Phys. Rev. D **72**, 053002 (2005).
[36] M. Ishitsuka *et al.*, Phys. Rev. D **72**, 033003 (2005); K. Hagiwara, N. Okamura and K. I. Senda, Phys. Lett. B **637**, 266 (2006).
[37] O. Mena, S. Palomares-Ruiz and S. Pascoli, Phys. Rev. D **73**, 073007 (2006).
[38] T. Kajita *et al.*, arXiv:hep-ph/0609286.
[39] J. Burguet-Castell *et al.*, Nucl. Phys. B **646**, 301 (2002).

[40] P. Huber, M. Lindner and W. Winter, Nucl. Phys. B **654**, 3 (2003).
[41] H. Minakata, H. Nunokawa and S. J. Parke, Phys. Rev. D **68**, 013010 (2003).
[42] V. Barger, D. Marfatia and K. Whisnant, Phys. Lett. B **560**, 75 (2003).
[43] K. Whisnant, J. M. Yang and B. L. Young, Phys. Rev. D **67**, 013004 (2003); P. Huber *et al.*, Nucl. Phys. B **665**, 487 (2003); P. Huber *et al.*, Phys. Rev. D **70**, 073014 (2004); A. Donini, E. Fernández-Martínez and S. Rigolin, Phys. Lett. B **621**, 276 (2005).
[44] O. Mena and S. J. Parke, Phys. Rev. D **70**, 093011 (2004).
[45] P. Huber, M. Maltoni and T. Schwetz, Phys. Rev. D **71**, 053006 (2005).
[46] S. Choubey and P. Roy, Phys. Rev. D **73**, 013006 (2006).
[47] A. Blondel *et al.*, Acta Phys. Polon. B **37**, 2077 (2006); A. Blondel, arXiv:hep-ph/0606111.
[48] O. Mena, H. Nunokawa and S. J. Parke, Phys. Rev. D **75**, 033002 (2007); O. Mena, arXiv:hep-ph/0609031.
[49] A. Jansson, O. Mena, S. J. Parke and N. Saoulidou, Phys. Rev. D **78**, 053002 (2008).
[50] P. Huber, M. Lindner and W. Winter, Comput. Phys. Commun. **167**, 195 (2005); P. Huber *et al.*, Comput. Phys. Commun. **177**, 432 (2007).
[51] IDS-NF Steering Group, IDS-NF-Baseline-2007/1.0 (2008).
[52] A. Donini *et al.*, Nucl. Phys. B **743**, 41 (2006).
[53] V. Barger *et al.*, FERMILAB-0801-AD-E, BNL-77973-2007-IR, FERMILAB-APC (2007), arXiv:0705.4396 (hep-ph); M. Diwan *et al.*, BNL-76798-2006-IR (2006), arXiv:hep-ex/0608023; V. Barger *et al.*, Phys. Rev. D **74**, 073004 (2006).
[54] J. N. Bahcall, M. Baldo-Ceolin, D. B. Cline and C. Rubbia, Phys. Lett. B **178**, 324 (1986).
[55] B. Fleming - private communication reported in Phys. Rev. D **76**, 053005 (2007).
[56] Y. Itow *et al.* [The T2K Collaboration], KEK-REPORT-2001-4, ICRR-REPORT-477-2001-7, TRI-PP-01-05 (2001), arXiv: hep-ex/0106019.
[57] P. Zucchelli, Phys. Lett. B **532**, 166 (2002).
[58] J. Burguet-Castell, D. Casper, E. Couce, J.J. Gomez-Cadenas and P. Hernandez, Nucl. Phys. B **725**, 306 (2005); J. Burguet-Castell, D. Casper, J.J. Gomez-Cadenas, P. Hernandez and F. Sanchez, Nucl. Phys. B **695**, 217 (2004).
[59] S. Choubey, P. Coloma, A. Donini and E. Fernández Martínez, arXiv:0907.2379 (hep-ph).